Available online at website: https://journal.bcrec.id/index.php/bcrec

Bulletin of Chemical Reaction Engineering & Catalysis, 19 (2) 2024, 252-264

Research Article

Optimization Photodegradation of Methylene Blue Dye using Bentonite/PDA/Fe_3O_4@CuO Composite by Response Surface Methodology

Fahma Riyanti[1], Poedji Loekitowati Hariani[2,3,*], H. Hasanudin[3], Addy Rachmat[2,3], Widia Purwaningrum[1]

[1]Doctoral Program of Mathematics and Natural Sciences, Faculty of Mathematics and Natural Sciences, Universitas Sriwijaya, Ogan Ilir 30662, Indonesia.
[2]Research Group on Magnetic Materials, Department of Chemistry, Faculty of Mathematics and Natural Sciences, Universitas Sriwijaya, Ogan Ilir 30662, Indonesia.
[3]Department of Chemistry, Faculty of Mathematics and Natural Sciences, Universitas Sriwijaya, Ogan Ilir 30662, Indonesia.

Received: 19th February 2024; Revised: 18th May 2024; Accepted: 21st May 2024
Available online: 11th June 2024; Published regularly: August 2024

Abstract

This study aims to synthesize bentonite/PDA/Fe_3O_4@CuO composites as a catalyst for the photodegradation of Methylene blue dye. Composite characterization involves X-ray Diffractometry (XRD), Scanning Electron Microscopy (SEM) with X-ray Energy Dispersion Spectrometry (EDS), UV-Vis Diffuse Reflectance Spectroscopy (UV-Vis DRS), and Vibrating Sample Magnetometer (VSM). Response Surface Methodology (RSM) employs Central Composite Design (CCD) to optimize photodegradation by varying dye concentration, irradiation time, and catalyst dose. The bentonite/PDA/Fe_3O_4@CuO composites exhibit a saturation magnetization value of 54.82 emu/g and a band gap of 2.1 eV. The optimization revealed that concentration and dose significantly impact the photodegradation efficiency. A quadratic model is suitable for modeling the photodegradation of Methylene blue dye using bentonite/PDA/Fe_3O_4@CuO composites, as determined by analysis of variance (ANOVA). The optimal conditions for achieving maximum photodegradation efficiency were identified as a dye concentration of 10 mg/L, an exposure time of 90 min, and a catalyst dose of 1.67 g/L. Under these parameters, the photodegradation process exhibited a remarkable efficiency of 100%. The Bentonite/PDA/Fe_3O_4@CuO composites exhibited strong stability, efficiency, and recyclability. After six photodegradation cycles, there was a 5.18% decrease in photodegradation efficiency.

Keywords: bentonite/PDA/Fe_3O_4@CuO; photodegradation; Methylene blue dye; RSM optimization; quadratic model

How to Cite: F. Riyanti, P.L. Hariani, H. Hasanudin, A. Rachmat, W. Purwaningrum (2024). Optimization Photodegradation of Methylene Blue Dye using Bentonite/PDA/Fe_3O_4@CuO Composite by Response Surface Methodology. *Bulletin of Chemical Reaction Engineering & Catalysis*, 19 (2), 252-264 (doi: 10.9767/bcrec.20132)

Permalink/DOI: https://doi.org/10.9767/bcrec.20132

1. Introduction

Toxic liquid waste containing dye chemicals threatens our natural ecosystem significantly. Most dye waste is non-biodegradable, carcinogenic, and poses significant risks to humans and aquatic animals [1]. Various industries, including textile, chemical, printing, cosmetics, photography, paper, plastic, and food, generate waste containing hazardous dyes [2,3]. Methylene blue dye is a commonly utilized dye in various industries. The molecular formula of methylene blue dye is $C_{16}H_{18}ClN_3S$. It is a cationic dye containing an aromatic amine group that poses a challenge due to its resistance to degradation [4,5].

Several techniques have been employed to decrease the level of Methylene blue dye prior to its release into the environment, such as adsorption [6], coagulation-flocculation [7], electrolysis [8], reverse osmosis [9], and advanced oxidation process [10]. The Advanced Oxidation

* Corresponding Author.
Email: puji_lukitowati@mipa.unsri.ac.id (P.L. Hariani)

process (AOP) shows excellent potential for treating waste with dyes [11,12]. Heterogeneous photocatalysis is an effective AOP technique for degrading dyes. Photocatalysis semiconductors are efficient and environmentally friendly, a promising technology for eliminating refractory pollutants from water [13]. Hydroperoxyl radicals, hydroxyl radicals, and superoxide ions contribute to the degradation of dyes into smaller, non-toxic molecules such as H_2O and CO_2 [14,15].

This study utilizes a composite material of metal oxide (MO-n) and bentonite. Metal oxides (MO-n), such as Copper oxide (CuO), are utilized in photocatalytic research due to their biocompatibility, stability, and cost-effectiveness [16]. CuO is a p-type transition metal semiconductor with a band gap energy of 1.2–1.5 eV, that can be used in the visible region [17]. However, CuO as a catalyst has a weakness, which lies in its susceptibility to agglomeration due to its small size, diminishing the efficiency of photocatalysis.

Bentonite is a type of clay known for its stability and large surface area, making it suitable for use as an adsorbent or catalyst [18]. Attaching Fe_3O_4 particles to bentonite enhances degradation efficiency and allows for easy separation of the catalyst from the solution using a magnet [19]. Fe_3O_4 is a non-toxic, biocompatible material with robust magnetic properties [20]. To ensure proper dispersion of the active catalyst species on a solid support, the surface must be altered using organic ligands like Polydopamine (PDA) [21]. PDA contains various functional groups, such as catechol and amino, which can bind strongly to organic and inorganic materials through hydrogen bonds [22]. For example, PDA can adsorb Pb metal ions and Methylene blue dye [23,24].

CuO has long been employed as a catalyst to enhance its performance, combined with other materials like bentonite/PDA/Fe_3O_4 to enhance the holes and photo-generated, separate electrons and prevent agglomeration. The composite is magnetic, making it easier to separate and regenerate. This research aims to synthesize a bentonite/PDA/Fe_3O_4@CuO composite. Fe_3O_4 as the bentonite pillar and imparts magnetic properties, with PDA serving as a layer and where CuO acts as a catalyst distributed on the bentonite/PDA/Fe_3O_4 surface [21]. A statistical approach was used to optimize the photodegradation process using Response Surface Methodology (RSM). The RSM is a reliable statistical technique for modeling to optimize and understand catalyst performance and verify the studied variables [25,26]. The photocatalytic activity of the composite towards Methylene blue dye includes the variables of dye concentration, contact time, and catalyst dose.

2. Materials and Methods

2.1 Material

Chemicals include $FeCl_3.6H_2O$, $FeSO_4.7H_2O$, NaOH, ethanol, $Cu(NO_3)_2$, dopamine (DA), Tris Chloride (TrisCl), and Methylene blue dye all sourced from Merck, Germany. Bentonite clay originates from Jambi province.

2.2 Bentonite Preparation

Natural bentonite was crushed and then screened through a 200-mesh sieve. The bentonite was then immersed in a 1% hydrochloric acid solution (bentonite to HCl ratio of 1:2) for 4 h. Bentonite was rinsed with distilled water until the pH was neutral and then dried in an oven at 105 °C for 6 h [19].

2.3 Synthesis of Bentonite/PDA

The bentonite/PDA synthesis followed the method Ain *et al*. [21]. A total of 5 g of prepared bentonite was added to 200 mL of distilled water and stirred for 30 min with a magnetic stirrer. Subsequently, 0.2 g of DA and 0.4 g of TrisCl were added, and stirring was maintained for 24 h. The bentonite/PDA composite was isolated from the solution through filtration and multiple washes with distilled water and ethanol. The Bentonite/PDA mixture was then dehydrated at 60 °C in an oven for 3 h.

2.4 Synthesis of Bentonite/PDA/Fe_3O_4

A total of 2 g of bentonite/PDA was added to 200 mL of a solution containing 0.745 g of $FeCl_3.6H_2O$ and 1.165 g of $FeSO_4.7H_2O$. The solution was stirred as NaOH with a concentration of 1 M was added slowly while nitrogen gas was flowing. The stirring continued for approximately 1 h until the solution reached a pH of ±11. The precipitate was rinsed with distilled water until it reached a neutral pH, then dried in an oven at 105 °C for 2 h.

2.5 Synthesis of Bentonite/PDA/Fe_3O_4@CuO

10 mL of a 0.02 M $Cu(NO_3)_2$ solution was treated with 1.16 g of bentonite/PDA/Fe_3O_4 composite. After 120 min of sonication, the mixture was thoroughly cleaned with distilled water and ethanol to bring its pH to neutral. The obtained precipitate was then dried at 70 °C for 2 h and subsequently calcined at 400 °C for 60 min.

2.6 Characterizations

X-ray Diffraction (XRD) analysis was conducted using a Cu-Kα radiation source (λ = 0.15418 Å) with a PANalytical XPERT PRO instrument, scanning in the 10 to 90° range to determine phase type and crystal size. Band gap

values were determined through UV-Vis Diffuse Reflectance Spectrometry (UV-Vis DRS) using a Hitachi U-2900 instrument. Scanning Electron Microscopy-Electron Dispersive X-ray Spectroscopy (SEM-EDS) with a JSM-6510 LA instrument was employed for morphological and elemental composition analyses. Magnetic properties were assessed using a Vibration Sample Magnetometer (VSM Oxford Type 1.2 H). Fourier Transform Infrared (FTIR) analysis of functional groups before and after photodegradation was performed using a Thermo Scientific Nicolet iS-10 instrument, with KBr pellets for sample presentation, in the 400-4000 cm^{-1} wave number range. UV-Vis Spectrophotometry (Orion Aquamate 8000) was utilized to measure the absorbance of Methylene blue dye.

2.7 Photocatalytic Activity Optimization

The photodegradation process for Methylene blue dye was optimized using RSM. The CCD model, implemented with Design-Expert software (Version 13), facilitated the experimental design. A total of 20 experiments were conducted, incorporating independent variables such as dye concentration, irradiation time, and catalyst dose. Visible light (60 watts, Philips lamps) was the radiation source. After completing all experiments, the appropriate model was analyzed to characterize the photodegradation of Methylene blue dye employing the bentonite/Fe_3O_4/PDA@CuO composite.

The catalyst undergoes regeneration in six cycles. In each regeneration step, the catalyst was extracted from the solution employing a permanent magnet, followed by a thorough washing process with distilled water and ethanol [27]. Subsequently, the catalyst is subjected to drying in an oven for 2 h at a temperature of 70 °C. The photodegradation efficiency was calculated from the decrease of dyes concentration measured by UV-Visible Spectrophotometer after irradiation treatment.

3. Results and Discussion

3.1 XRD Analysis

Figure 1 illustrates the spectra of bentonite, bentonite/PDA, bentonite/Fe_3O_4/PDA, and bentonite/Fe_3O_4/PDA@CuO. The major peaks indicating the presence of bentonite at 2θ = 20.22°, 21.26°, 27.15°, and 50.18°, aligning with the findings of Wan et al. [28], reported peaks at 2θ = 20.4°, 21.3°, 27.2°, and 50.53°. The spectra of bentonite/PDA exhibit similarities to those of bentonite but with reduced intensity, attributed to the introduction of PDA, an organic compound [29]. The spectra of bentonite/Fe_3O_4/PDA exhibit diminished intensity compared to bentonite and bentonite/PDA, featuring characteristic Fe_3O_4 peaks at 30.25°, 35.62°, 43.46°, 54.21°, 57.43°, and 63.18° corresponding to JCPDS card No. 75-0449.

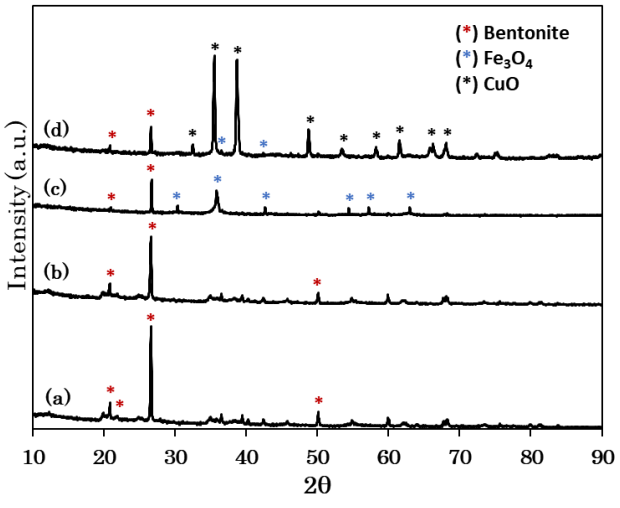

Figure 1. XRD pattern of (a) bentonite, (b) bentonite/PDA, (c) bentonite/Fe_3O_4/PDA, and (d) bentonite/Fe_3O_4/PDA@CuO.

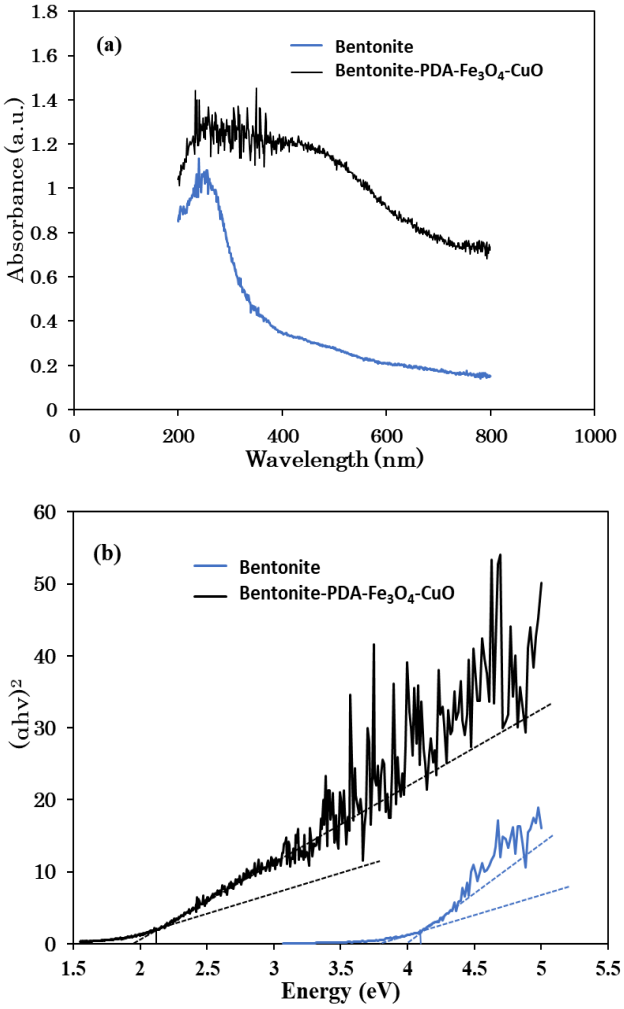

Figure 2. Spectra of (a) UV-Vis DRS and (b) Band gap energies of bentonite and bentonite/Fe_3O_4/PDA@CuO.

In bentonite/Fe_3O_4/PDA@CuO, the presence of CuO is evident through sharp and intense peaks at $2\theta = 32.44^o$, 35.54^o, 38.66^o, 48.83^o, 53.66^o, 58.24^o, 61.59^o, 66.30^o, and 68.14^o, associated with crystal planes (110), (002), (111), (112), (020), (202), (113), and (220), corresponding to JCPDS card No. 89-5895. Gomaa et al. [30] reported on his work in accordance with JCPDS Card No. 89-5895. The average crystal sizes, determined using the Debye Scherrer equation, were 23.6, 25.8, 27.4, and 31.4 nm for bentonite, bentonite/PDA, bentonite/Fe_3O_4/PDA, and bentonite/Fe_3O_4/PDA@CuO, respectively.

3.2 UV-DRS Analysis

UV-DRS spectroscopy assessed the band gap energy of both bentonite and the bentonite/Fe_3O_4/PDA@CuO composites. In Figure 2(a), the UV-DRS spectrum of bentonite exhibits a distinct absorption peak at approximately 263 nm, whereas the bentonite/Fe_3O_4/PDA@CuO composite displays a broader peak spanning 400-500 nm. This absorption is primarily influenced by the presence of Fe_3O_4 and CuO in the visible region [31]. CuO, being a direct band semiconductor, efficiently absorbs light within the 400-580 nm wavelength range [32]. The band gap energy is the amount of energy necessary to move electrons from the valence band to the conduction band in a semiconductor material. Calculating the estimated band gap energy value involves the application of the following equation [33,34].

$$(\alpha h\upsilon)^n = A(h\upsilon - E_g) \quad (1)$$

The symbol α represents the absorption coefficient, $h\upsilon$ denotes photon energy, and n characterizes the type of transition (1/2 or 2, representing direct and indirect transitions, respectively). A represents a constant and E_g stands for the band gap energy. The determination of E_g involves plotting of $(\alpha h\upsilon)^2$ against $h\upsilon$. The linear region indicating an indirect band gap.

The Tauc function plots reveal band gap energies of 4.1 eV and 2.1 eV for bentonite and bentonite/Fe_3O_4/PDA@CuO composites, respectively (Figure 2(b)). The band gap value is obtained from the intersection point of the tangent line to the horizontal axis [35]. This discrepancy

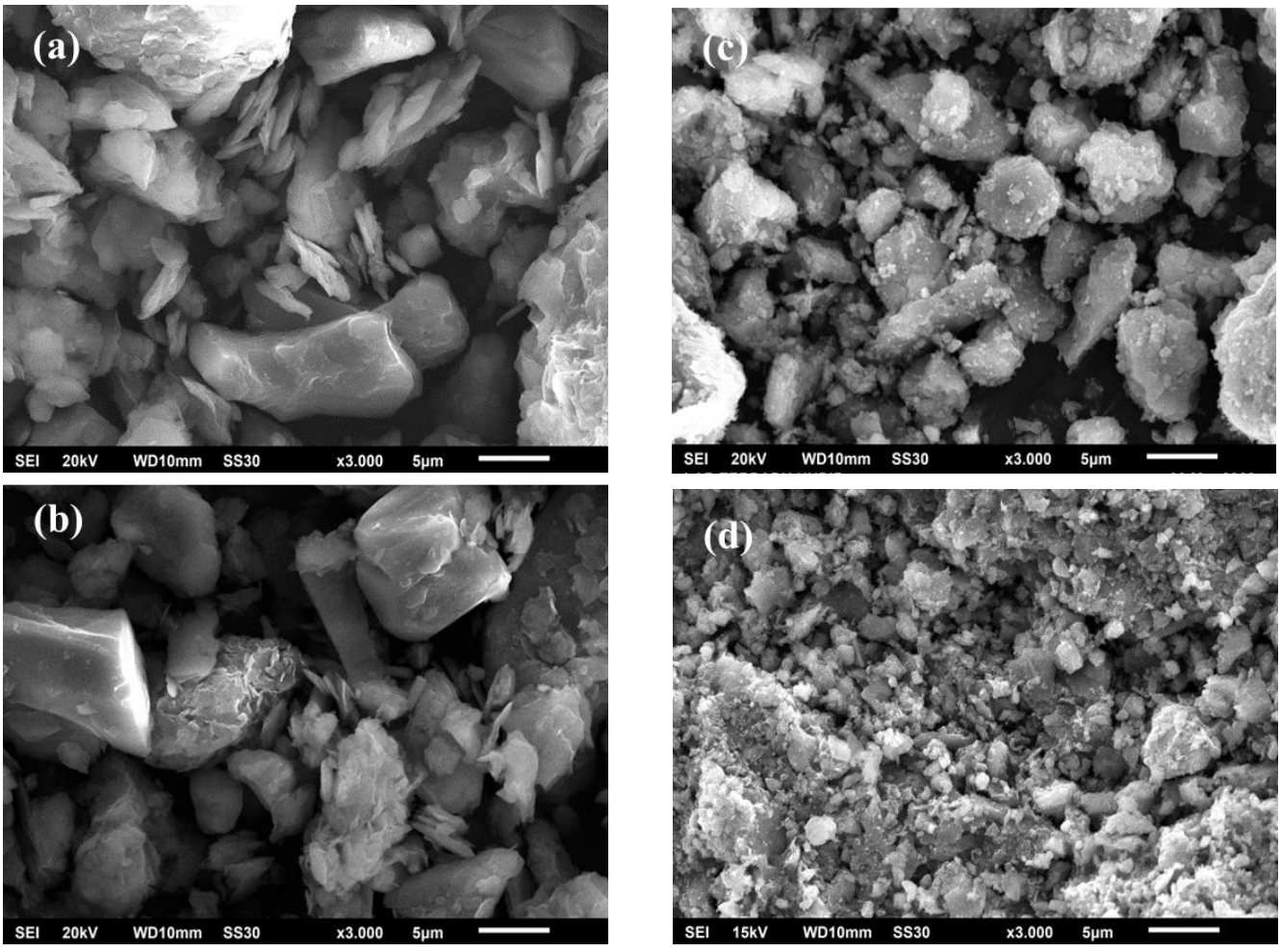

Figure 3. Morfologi (a) bentonite, (b) bentonite/PDA, (c) bentonite/Fe_3O_4/PDA dan (d) bentonite/Fe_3O_4/PDA@CuO.

in the energy band gap is attributed to the presence of a p-n heterojunction on the catalyst. Furthermore, the incorporation of Fe_3O_4 and CuO into the composite results in a reduction of the energy band gap. Additionally, introducing Fe_3O_4 and CuO facilitates enhanced transfer and separation of electron-hole pairs, leading to improved photocatalytic activity [31].

3.3 SEM-EDS Analysis

The surface characteristics were observed via SEM, while the elemental composition was analyzed using EDS assessment. Figure 3 depicts the structural features of bentonite, bentonite/PDA, bentonite/Fe_3O_4/PDA, and bentonite/Fe_3O_4/PDA@CuO. Jiang *et al*. [36] reported that bentonite showcases a layered configuration. Both bentonite/PDA and bentonite/Fe_3O_4/PDA show heterogeneous surfaces. The bentonite/Fe_3O_4/PDA surface appears denser and there are small chunks between the layers indicating the presence of Fe_3O_4. The bentonite/Fe_3O_4/PDA@CuO composite manifests minute, dispersed grains on its surface, indicating CuO dispersed on the surface of bentonite/Fe_3O_4/PDA.

Table 1 presents the elemental composition of bentonite, bentonite/PDA, bentonite/Fe_3O_4/PDA, and bentonite/Fe_3O_4/PDA@CuO. Bentonite exhibits a composition containing various elements, including C, O, Na, Al, Fe, and K. Upon introducing PDA, there is a discernible increase in the carbon percentage. The percentage of Fe is increased when Fe_3O_4 is added to bentonite/PDA. The amount of Cu in the bentonite/Fe_3O_4/PDA/CuO composite is 16 wt.%, indicating that the composite contains CuO.

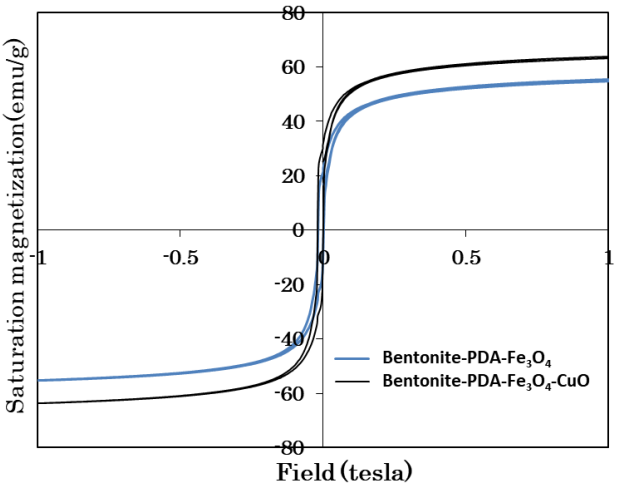

Figure 4. Magnetic hysteresis loops of bentonite/Fe_3O_4/PDA dan bentonite/Fe_3O_4/PDA@CuO.

3.4 VSM Analysis

The examination of magnetic properties through hysteresis loop curves is presented in Figure 4 for bentonite/Fe_3O_4/PDA and bentonite/Fe_3O_4/PDA@CuO. Bentonite and bentonite/PDA exhibit no magnetic characteristics. Notably, the magnetic properties of bentonite/Fe_3O_4/PDA surpass those of bentonite/Fe_3O_4/PDA@CuO, with a saturation magnetization value of 63.27 emu/g compared to 54.82 emu/g. The introduction of nonmagnetic components leads to a reduction in magnetic properties [37]. Similar trends are observed in other studies, where Fe_3O_4/PDA demonstrates a higher saturation magnetization than MnO_2/PDA/Fe_3O_4 [38]. The S-shaped loop on the curve indicates superparamagnetic behavior [21]. The magnetic properties of bentonite/Fe_3O_4/PDA@CuO enable the rapid separation of the photocatalyst from the solution post-catalysis using a permanent magnet without filtration.

3.5 Photodegradation of Methylene Blue Dye

In the process of photodegradation involving Methylene blue dye and the bentonite/PDA/Fe_3O_4@CuO composite, various parameters, including concentration (mg/L), time irradiation (min), and dose (g/L), were systematically examined. The optimization procedure was carried out using RSM with CCD models. A total of 20 randomized experiments were designed to acquire both experimental and predicted photodegradation efficiency, as outlined in Table 2. Discrepancies between experimental and predicted data serve as a means to assess the precision and validity of the RSM model.

Table 1. Elemental composition of bentonite, bentonite/PDA, bentonite/Fe_3O_4/PDA dan bentonite/Fe_3O_4/PDA@CuO.

Materials	Elements (wt.%)							
	C	O	Na	Al	Si	Fe	K	Cu
Bentonite	9.75	56.85	1.25	7.63	22.78	1.22	0.52	-
Bentonite/PDA	31.50	35.80	-	6.94	24.08	1.24	0.44	-
Bentonite/PDA/Fe_3O_4	28.61	32.75	-	3.65	7.32	27.40	0.27	-
Bentonite/PDA/Fe_3O_4@CuO	27.07	30.69	-	2.80	5.80	17.13	-	16.51

The optimal conditions for the photodegradation process were determined to be a Methylene blue dye concentration of 10 mg/L, an irradiation time of 10 min, and a composite dose of 1.67 g/L. The photodegradation efficiency under these conditions was 100%, while the predicted value was 99.76%. The difference of only 0.24% attests to the concurrence between the experimental and predicted data, affirming the accuracy of the RSM model.

Figure 5 displays the comparison between predicted and actual photodegradation efficiency. The average residual value, standing at 0.685 and in proximity to zero, indicates normal scattering.

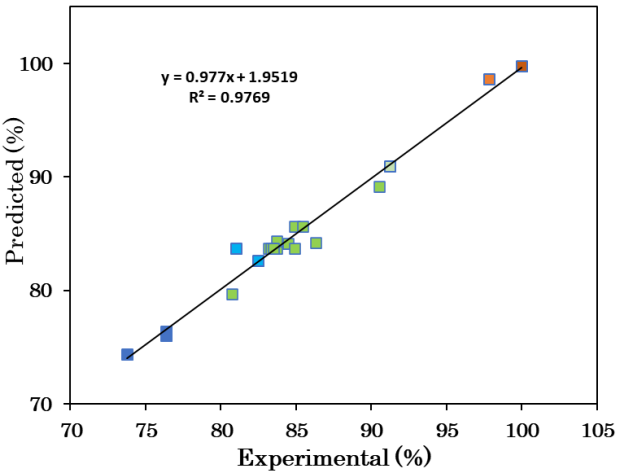

Figure 5. The plot of predicted versus experiment (values) for photodegradation of Methylene blue dye by bentonite/PDA/Fe_3O_4@CuO

This observation leads to the conclusion that the residual achieved is within the expected ranges, affirming the suitability of the proposed model [39].

The photodegradation process of Methylene blue dye encompasses the following phases. Initially, the bentonite/PDA/Fe_3O_4@CuO catalyst absorbs radiation energy, facilitating the excitation of electrons from the valence band (VB) to the conduction band (CB). This transition results in the generation of holes (h^+), which subsequently interact with H_2O, leading to the formation of $\cdot OH$ and $\cdot O_2^-$ species. These species actively contribute to the degradation of the dye, yielding non-harmful byproducts like H_2O and CO_2 [27,40]. Equations (2) – (8) show the photodegradation mechanism of Methylene blue dye using bentonite/PDA/Fe_3O_4@CuO [40,41].

$$\text{Bentonite/ } Fe_3O_4\text{/ PDA@CuO} + h\upsilon \rightarrow \text{Bentonite/ } Fe_3O_4\text{/ PDA@CuO}\left(e_{CB}^- + h_{VB}^+\right) \quad (2)$$

$$h_{VB}^+ + OH^- \rightarrow \cdot OH \quad (3)$$

$$e_{CB}^- + O_2 \rightarrow \cdot O_2^- \quad (4)$$

$$\cdot O_2^- + H_2O \rightarrow \cdot HO_2 + OH^- \quad (5)$$

$$\cdot HO_2 + \cdot HO_2 \rightarrow H_2O_2 + O_2 \quad (6)$$

$$H_2O_2 + \cdot O_2^- \rightarrow \cdot OH + OH^- + O_2 \quad (7)$$

$$\cdot OH + \cdot O_2^- + MB \rightarrow \text{Degradation product} \rightarrow CO_2 + H_2O + \text{other product} \quad (8)$$

Table 2. Experimental and predicted photodegradation of Methylene blue dye utilizing bentonite/PDA/Fe_3O_4@CuO

Run	Concentration (mg/L)	Time (min)	Dose (g/L)	Photodegradation efficiency (%)		Residual
				Experimental	Predicted	
1	10	10	0.33	82.49	82.62	-0.13
2	30	50	0.33	76.36	76.38	-0.02
3	10	90	0.33	84.47	84.16	0.31
4	50	90	0.33	76.37	75.97	0.40
5	30	90	1	84.89	85.66	-0.77
6	50	50	1	80.71	79.73	0.98
7	30	50	1	83.18	83.70	-0.52
8	10	90	1.67	100	99.76	0.24
9	30	50	1	84.89	83.70	1.19
10	30	50	1.67	90.51	89.21	1.30
11	30	50	1	83.73	83.70	0.03
12	10	10	1.67	97.85	98.58	-0.73
13	50	10	1.67	83.73	84.36	-0.63
14	10	50	1	91.23	90.93	0.39
15	30	50	1	83.34	83.70	-0.36
16	30	10	1	86.29	84.24	2.05
17	50	90	1.67	85.45	85.64	-0.19
18	50	10	0.33	73.76	74.32	-0.56
19	30	50	1	83.47	83.70	-0.23
20	30	50	1	81.03	83.70	-2.67

Notably, the PDA component, enriched with quinone rings, is pivotal in efficiently transporting electrons and holes between donors and acceptors. Furthermore, the catechol group within PDA serves as a two-electron gate, significantly enhancing electron transfer efficiency [42,43]. Figure 6 explains the photodegradation mechanism of Methylene blue dye.

The photodegradation of Methylene blue dye produces water (H_2O), carbon dioxide (CO_2), and other products. These other products could basic non-toxic organic acids like acetic acid and oxalic acid, as well as mineralized inorganic substances such as nitrates, sulfites, and sulfates [44]. Other studies indicate that 40% of methylene blue dye undergoes mineralization, while the remaining portion is oxidized into smaller molecular substances like propionic acid and malonic acid [45].

Through the ANOVA analysis, we have examined the interplay of various variables within the photodegradation process. As per the following equation, the quadratic model is the preferred model for representing this degradation process.

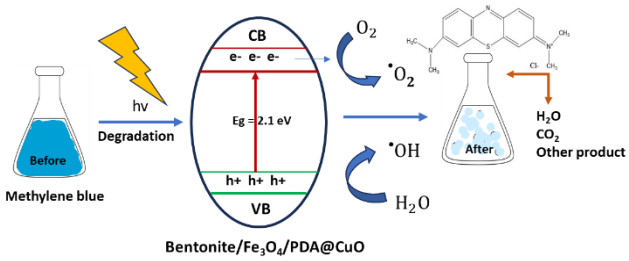

Figure 6. The schematic for the photodegradation of Methylene blue dye.

$$Y = 81.82495 - 0.415715A - 0.058054B + 17.07909C + 0.00031AB - 0.110448AC - 0.003358BC + 0.004075A^2 + 0.000781B^2 - 2.01604C^2 \quad (9)$$

A, B, and C correspond to concentration, irradiation time, and dose in the investigation of photodegradation. The suitability of the quadratic model was assessed through ANOVA, including F-value, P-value, and Lack of Fit. A quadratic model was also produced for the photodegradation of Methylene blue utilizing g-C_3N_4 [46] and Zn-La oxide [47]. The varying p values suggest that not all variables play a significant role in photodegradation. Table 3 displays the ANOVA results for the quadratic model analysis of methylene blue dye photodegradation.

With a model F-value of 47.09, it is evident that the model holds significance. The likelihood of the F-value occurring due to noise is a mere 0.01%, reinforcing the model's robustness. A P-value below 0.05 further confirms the model's significance. The variables that exhibit significant influence based on their P-values are concentration and dose, while time does not demonstrate a significant impact on the photodegradation process of methylene blue dye. Increasing the dye concentration and catalyst doses indeed impacts the extent of degradation. However, elevated dye concentrations can hinder

Table 3. Analysis of variance for quadratic models.

Source	Sum of squares	Degree of freedom	Mean of Square	F-value	P-value	
Model	768.93	9	85.44	47.09	< 0.0001	Significant
A-Concentration	313.82	1	313.82	172.95	< 0.0001	
B-Times	4.98	1	4.98	2.75	0.1284	
C-Doses	410.75	1	410.75	22	< 0.0001	
AB	0.0050	1	0.0050	0.0028	0.9592	
AC	17.52	1	17.52	9.66	0.0111	
BC	0.0648	1	0.0648	0.0357	0.8539	
A^2	7.31	1	7.31	4.03	0.0726	
B^2	4.30	1	4.30	2.37	0.1549	
C^2	2.25	1	2.25	1.24	0.2913	
Residual	18.15	10	1.81	-	-	
Lack of Fit	10.24	5	2.05	1.29	0.3918	Non-significant
Pure error	7.91	5	1.58	-	-	
Std. Dev	-	-	-	-	-	1.32
Mean	-	-	-	-	-	84.69
CV %	-	-	-	-	-	1.59
R^2	-	-	-	-	-	0.9769
Adjusted R^2	-	-	-	-	-	0.9562
Predicted R^2	-	-	-	-	-	0.9004
Adeq Precision	-	-	-	-	-	26.7024

light penetration onto the catalyst, limiting the generation of active species necessary for dye degradation. Similarly, at higher catalyst doses, while the number of active species may increase, turbidity can develop, impeding light penetration. Consequently, optimizing photodegradation variables becomes crucial to strike a balance and achieve optimal degradation efficiency [48].

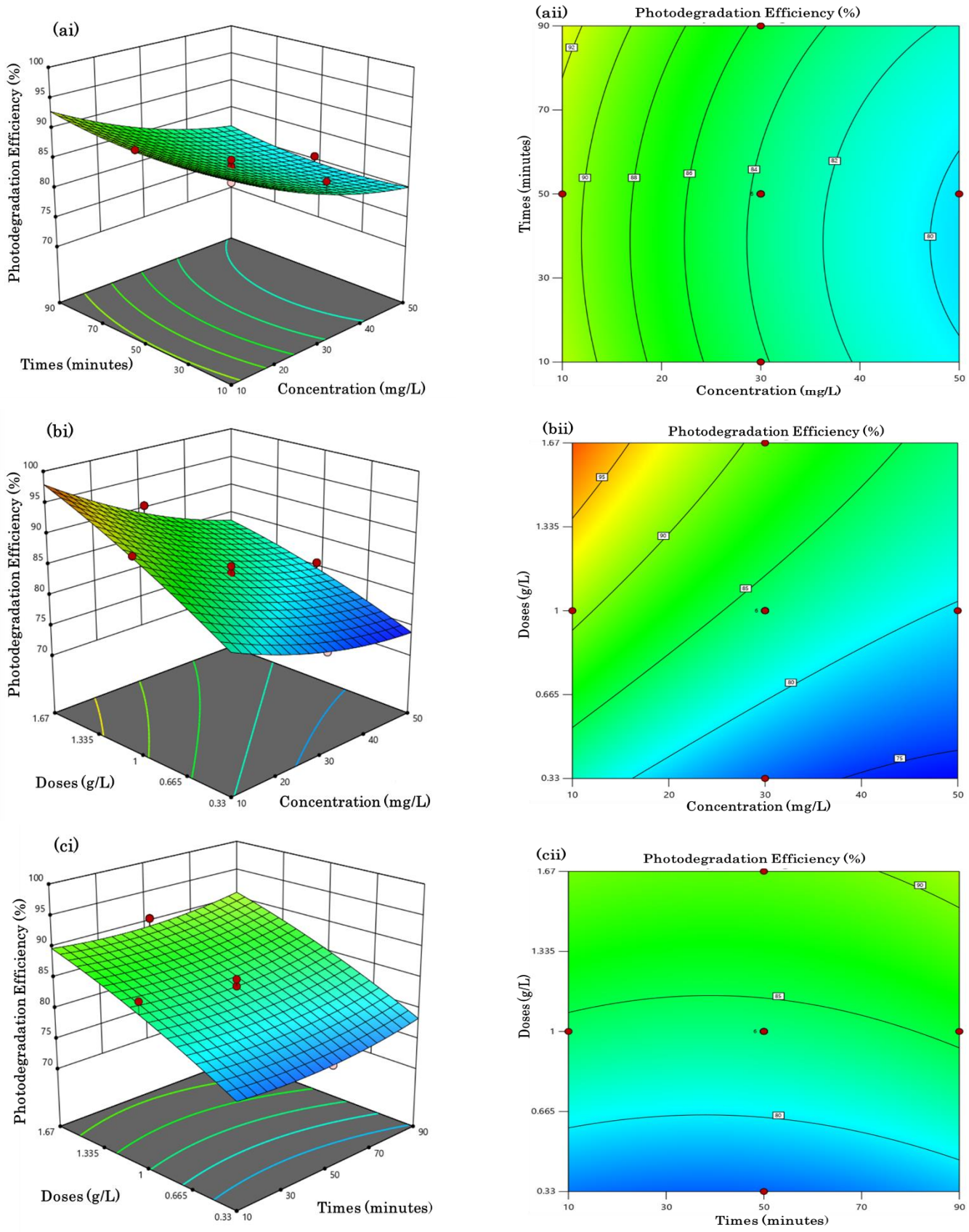

Figure 7. Response surface and contour plots of the effect a) times and concentration, b) doses and concentration, and c) doses and times.

This aligns with related research, such as the photodegradation of Rhodamine B dye using Bi-metal doped TiO_2 [49] and the photodegradation of Methyl orange dye using cellulose/zinc oxide hybrid air gel [50], both employing the quadratic model. The lack of fit F-value of 1.29 implies the lack of fit is not significant relative to the pure error. There is a 39.18% change that a lack of fit F-value could occur due to noise. A non-significant lack of fit is good, as it indicates that the model fits the data well.

The obtained linear regression coefficient (R^2) value is 0.9769, closely approaching 1. This proximity suggests a strong correspondence between the experimental and predicted responses. The marginal difference between the adjusted R^2 (0.9562) and predicted R^2 (0.9004), both being less than 0.2, signifies the capability of the model [51]. The optimal conditions zone is determined by assessing interaction variations as a response function, specifically in photodegradation efficiency. Figure 7 illustrates the 3D surface response and contour plots portraying the photodegradation efficiency of Methylene blue dye using Bentonite/Fe_3O_4/PDA@CuO composites, with dye concentration, irradiation time, and dose variations.

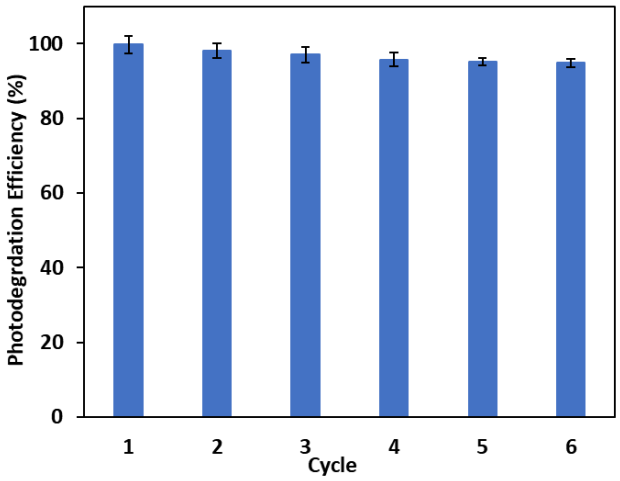

Figure 8. Recyclability test for photodegradation of Methylene blue dye.

The optimum conditions for photodegradation were obtained at the Methylene blue dye concentration (10 mg/L), dose (1.67 g/L), and irradiation time (90 min). Concentration has a negative effect on photodegradation efficiency. As the concentration of Methylene blue dye increases, the photodegradation efficiency decreases. Increasing the dye concentration blocks radiation energy from reaching the catalyst [52]. Increasing the dose of the bentonite/PDA/Fe_3O_4@CuO composite enhances photodegradation efficiency because more catalyst generates a greater amount of $\cdot OH$ and $\cdot O_2^-$ to radicals to break down the dye.

Table 4 is a comparison of catalysts for photodegradation of Methylene blue dye. Even though the dose used in this research is quite large, compared to other researchers. However, the photodegradation using this composite is an efficient process because the composite can be separated from the solution quickly after the degradation process using an external magnet without filtering. It can be seen that bentonite/PDA/Fe_3O_4@CuO composite has greater photodegradation efficiency for Methylene blue dye than some catalysts.

3.6 Photocatalyst Recyclability

The bentonite/PDA/Fe_3O_4@CuO regeneration process was conducted through six regeneration cycles. As depicted in Figure 8, the degradation efficiency experiences only a marginal reduction of 5.18% over the six regeneration cycles, affirming the catalyst's commendable stability. The decline in catalyst performance can be attributed to the potential blockage of active sites caused by dyes that persist after regeneration. This blockage impedes the diffusion of dye molecules to the surface of the photocatalyst [61,62]. Notably, the regeneration outcomes for Methylene blue dye in

Table 4. Photodegradation of several catalysts against Methylene blue dye.

Catalyst	Dose (g/L)	Concentration (mg/L)	Time (min)	Photodegradation (%)	Ref.
TiO_2-Fe_3O_4-Bentonite	0.3	40	90	90	[53]
MnO_2/bentonite	0.02	20	120	87	[54]
CeO/CuO	1.0	0.03	150	85.66	[55]
Zeolitic Imidazolate Framework-8	2	6	180	93.00	[56]
$NiFe_2O_4$/NiO	0.025	5	120	95.41	[57]
TiO_2-P25	0.125	10	300	60	[58]
B/P-carbons dots	0.05	10	60	92.3	[59]
Bentonite-Fe_3O_4	0.25	0.05	90	94.34	[19]
CeO_2-NPs	0.25	5	90	90	[60]
Bentonite/PDA/Fe_3O_4/CuO	1.67	10	90	100	This work

this study surpass those achieved with TiO_2-Fe_3O_4-Bentonite (20% reduction over six cycles) [53] and $SnWO_4$/ZnO (5.57% reduction over five cycles) [63].

4. Conclusions

This study successfully synthesized a magnetic bentonite/PDA/Fe_3O_4@CuO composite. The optimization of photodegradation was conducted using the RSM method with CCD, incorporating variables such as dye concentration, exposure time, and catalyst dose. The analysis results indicate a strong match between experimental data and predicted (R^2 = 0.9769), confirming adherence to the quadratic model. Maximum photodegradation efficiency (100%) was achieved under specific conditions: a Methylene blue dye concentration of 10 mg/L, an irradiation time of 90 min, and a catalyst dose of 1.67 g/L. The magnetic properties of this composite offer the advantage of facilitating the separation process. The catalyst demonstrates outstanding stability and can be regenerated for repeated use. The considerable efficacy of the catalyst in breaking down dyes holds promise for its application in wastewater containing dye compounds.

Acknowledgment

The research was supported by a grant awarded by Sriwijaya University through the Hibah Profesi Program, with Contract Number 0187/UN9.3.1/SK/2023, on April 18, 2023.

Credit Author Statement

Author contribution: Riyanti, F and Purwaningrum, W: Investigation, resources, Experiment and data analysis, Hariani, P.L: Conceptualization, writing, experiment and data analysis, Hasanudin: Methodology, experiment and data analysis, Rachmat, A: Review, editing and validation. All authors have read and agreed to the published version of the manuscript.

References

[1] Karuppusamy, I., Samuel, M.S., Shanmugam, S., Kumar, P.S.M.K., Brindhadevi, K., Pugazhendhi, A. (2021). Ultrasound-assisted synthesis of mixed calcium magnesium oxide ($CaMgO_2$) nanoflakes for photocatalytic degradation of Methylene blue. *Journal of Colloid and Interface Science*, 584(15), 770-778. DOI: 10.1016/j.jcis.2020.09.112

[2] Berhanu, S., Gebremariam, H., Chufamo, S. (2022). The g-C_3N_4@CdO/ZnO ternary composite: photocatalysis, thermodynamics and acute toxicity studies. *Heliyon*, 8, 1-9. DOI: 10.1016/j.heliyon.2022.e11612

[3] Razaghi, P., Dashtian, K., Yousefi, F., Karimi, R., Ghaedi, M. (2021). Gold anchoring to $CuFe_2F_8(H_2O)_2$ oxyfluoride for robust sono-photodegradation of Rhodamine-B. *Journal of Cleaner Production*, 313, 1-11. DOI: 10.1016/j.jclepro.2021.127916

[4] Ibrahim, A.A., Salama, R.S., El-Hakam, S.A., Khder, A.S., Ahmed, A.I. (2021). Synthesis of sulfated zirconium supported MCM-41 composite with high-rate adsorption of Methylene blue and excellent heterogeneous catalyst. *Colloids and Surfaces A: Physicochemical and Engineering Aspects*, 616, 1-11. DOI: 10.1016/j.colsurfa.2021.126361

[5] Han, F., Kombala, V.S.R., Srinivasan, M., Rajarathnam, D., Naidu, R. (2009). Tailored titanium dioxide photocatalysts for the degradation of organic dyes in wastewater treatment: A review. *Applied Catalys A: General*, 359(1-1), 25-40. DOI: 10.1016/j.apcata.2009.02.043

[6] Allou, N.B., Tigori, M.A., Koffi, A.A., Halidou, M., Eroi, N.S., Atheba, P., Trokourey, A. (2023). Methylene blue magnetic adsorption separation process from aqueous solution using corn cob. *Scientific African*, 21, 1-13. DOI: 10.1016/j.sciaf.2023.e01828

[7] Ihaddaden, S., Aberkane, D., Boukerroui, A., Robert, D. (2022). Removal of methylene blue (basic dye) by coagulation-flocculation with biomaterials (bentonite and *Opuntia ficus indica*). *Journal of Water Process Engineering*, 49, 1-12. DOI: 10.1016/j.jwpe.2022.102952

[8] Liu, L., He, D., Pan, F., Huang, R., Lin, H., Zhang, X. (2020). Comparative study on treatment of Methylene blue dye wastewater by different internal electrolysis systems and COD removal kinetics, thermodynamics and mechanism. *Chemosphere*, 238, 1-9. DOI: 10.1016/j.chemosphere.2019.124671

[9] Chen, H., Zhang, X., Shen, C., Wang, Y., Li, Z., CaO, B., Wang, S. (2023). Non-thermal plasma degradation of dye wastewater assisted by reverse osmosis process through interfacial mass transfer enhancement. *Chemical Engineering Science*, 282, 1-9. DOI: 10.1016/j.ces.2023.119221

[10] Mahamud, M., Taddesse, A.M., Bogale, Y., Bezu, Z. (2023). Zeolite supported CdS/TiO_2/CeO_2 composite: Synthesis, characterization and photocatalytic activity for Methylene blue dye degradation. *Materials Research Bulletin*, 161, 1-11. DOI: 10.1016/j.materresbull.2023.112176

[11] Vignesh, S., Chandrasekaran, S., Srinivasan, M., Anbarasan, R., Perumalsamy, R., Arumugam, E., Shkir, M., Alqarni, H., Alfaify, S. (2022). TiO_2-CeO_2/g-C_3N_4 S-scheme heterostructure composite for enhanced photo-degradation and hydrogen evolution performance with combined experimental and DFT study. *Chemosphere*, 288, 1-11. DOI: 10.1016/j.chemosphere.2021.132611

[12] Jaramillo-Fierro, X., Gonzalez, S., Montesdeoca-Mendoza, F., Medina, F. (2021). Structuring of $ZnTiO_3/TiO_2$ adsorbents for the removal of Methylene blue, using zeolite precursor clays as natural additives. *Nanomaterials*, 11(4), 1-25. DOI: 10.3390/nano11040898

[13] Hassani, A., Krishnan, S., Scaria, J., Eghbali, P., Nidheesh, P.V. (2021). Z-scheme photocatalysts for visible-light-driven pollutants degradation: A review on recent advancements. *Current Opinion in Solid State and Materials Science*, 25, 1-25. DOI: 10.1016/j.cossms.2021.100941

[14] Shehzad, N., Zafar, M., Ashfaq, M., Razzag, A., Akhter, P., Ahmad, N., Hafeez, A., Azam, K., Hussain, M., Kim, W.Y. (2020). Development of $AgFeO_2/rGO/TiO_2$ Ternary composite photocatalysts for enhanced photocatalytic dye decolorization. *Crystals*, 10(10), 1-15. DOI: 10.3390/cryst10100923

[15] Benalioua, B., Mansour, M., Bentouami, A., Boury, B., Elandaloussi, E.H. (2015). The layered double hydroxide route to Bi–Zn co-doped TiO_2 with high photocatalytic activity under visible light. *Journal of Hazardous Materials*, 288, 158-167. DOI: 10.1016/j.jhazmat.2015.02.013

[16] George, A., Raj, D.M.A., Venci, X., Raj, A.D., Irudayaraj, A.A., Josephine, R.L., Sundaram, S.J., Al-Mohaimeed, A.M., Farraj, D.A.A., Chen, T., Kaviyasarasu, K. (2022). Photocatalytic effect of CuO nanoparticles flower-like 3D nanostructures under visible light irradiation with the degradation of Methylene blue (MB) dye for environmental application. *Environmental Research*, 203, 1-6. DOI: 10.1016/j.envres.2021.111880

[17] Uma, H.B., Kumar, M.S.V., Ananda, S. (2022). Semiconductor-assisted photodegradation of textile dye, photo-voltaic and antibacterial property of electrochemically synthesized Sr-doped CuO nano photocatalysts. *Journal of Molecular Structure,* 1264, 1-10. DOI: 10.1016/j.molstruc.2022.133110

[18] Selvakumar, K., Raja, A., Arunpandian, M., Stalindurai, K., Rajasekaran, P., Sami, P., Nagarajan, E.R. (2019), Efficient photocatalytic degradation of ciprofloxacin and bisphenol A under visible light using Gd_2WO_6 loaded ZnO/bentonite nanocomposite. *Applied Surface Science*, 481, 1109-1119. DOI: 10.1016/j.apsusc.2019.03.178

[19] Riyanti, F., Hasanudin, H., Rachmat, A., Purwaningrum, W., Hariani, P.L. (2023). Photocatalytic degradation of Methylene blue and Congo red dyes from aqueous solutions by bentonite-Fe_3O_4 magnetic. *Communications in Science and Technology*, 8(1), 1-9. DOI: 10.21924/cst.8.1.2023.1007

[20] Khan, M., Tahir, N., Zahid, M., Yaseen, M., Jillani, A., Shakoor, R.A., Abbas, Q., Shahid, I. (2023). Visible light assisted photocatalytic degradation of methylene blue using iodine doped Fe_3O_4-GO composite. *Optik - International Journal for Light and Electron Optics*, 290, 1-18. DOI: 10.1016/j.ijleo.2023.171282

[21] Ain, Q.U., Rasheed, U., Yaseen, M., Zhang, H., Tomg, Z. (2020). Superior dye degradation and adsorption capability of polydopamine modified Fe_3O_4-pillared bentonite composite. *Journal of Hazardous Materials*, 397, 1-17. DOI: 10.1016/j.jhazmat.2020.122758

[22] Yang, D., Huang, S., Ruan, M., Li, S., Yang, J., Wu, Y., Guo, W., Zhang, L. (2018). Mussel inspired modification for aluminum oxide/silicone elastomer composites with largely improved thermal conductivity and low dielectric constant. *Industrial & Engineering Chemistry Research*, 57(9), 3255-3262. DOI: 10.1021/acs.iecr.7b04970

[23] Yang, W., Wang, Y., Wang, Q., Wu, J., Duan, G., Xu, W., Jian, S. (2021). Magnetically separable and recyclable Fe_3O_4@PDA covalent grafted by L-cysteine core-shell nanoparticles toward efficient removal of Pb^{2+}. *Vacuum*, 189, 1-10. DOI: 10.1016/j.vacuum.2021.110229

[24] Zhou, G., Wang, Q., Song, R., Li, S., Yang, S., Zhang, Q. (2023). Synthesis of core-double-shell structured Fe_3O_4@PDA/HKUST-1: Characterization analysis and adsorption performance on cationic MB dyes. *Journal of Physics and Chemistry of Solids*, 172, 1-11. DOI: 10.1016/j.jpcs.2022.111094

[25] Azzoumi, D., Baragh, F., Mahmoud, A.M., Alanazi, M.M., Rais, Z., Taleb, M. (2023). Optimization of Methylene blue removal from aqueous solutions using activated carbon derived from coffee ground pyrolysis: A response surface methodology (RSM) approach for natural and cost-effective adsorption. *Journal of Saudi Chemical Society*, 27, 1-17. DOI: 10.1016/j.jscs.2023.101695

[26] Mokhtar, A., Abdelkrim, S., Boukoussa, B., Hachemaoui, M., Djelad, A., Sassi, M., Abboud, M. (2023). Elimination of toxic azo dye using a calcium alginate beads impregnated with NiO/activated carbon: Preparation, characterization and RSM optimization. *International Journal of Biological Macromolecules*, 233, 1-13. DOI: 10.1016/j.ijbiomac.2023.123582

[27] Hariani, P.L., Salni, S., Said, M., Farahdiba, R. (2023). Core-shell $Fe_3O_4/SiO_2/TiO_2$ magnetic modified Ag for the photocatalytic degradation of Congo red dye and antibacterial activity. *Bulletin of Chemical Reaction Engineering & Catalysis*, 18(2), 315-330. DOI: 10.9767/bcrec.19275

[28] Wan, D., Wang, G., Li, W., Wei, X. (2017). Applied surface science investigation into the morphology and structure of magnetic bentonite nanocomposites with their catalytic activity. *Applied Surface Science*, 413, 398-407. DOI: 10.1016/j.apsusc.2017.03

[29] Ajibade, T.F., Tian, H., Lasisi, K.H., Zhang, K. (2022). Bio-inspired PDA@WS_2 polyacrylonitrile ultrafiltration membrane for the effective separation of saline oily wastewater and the removal of soluble dye. *Separation and Purification Technology*, 299, 1-15. DOI: 10.1016/j.seppur.2022.121711

[30] Gomaa, H., Hussein, M.A.T., Motawea, M.M., Aboraia, A.M., Cheira, M.F., Alotaibi, M.T., El-Bahy, S.M., Ali, H.M. (2022). A hybrid mesoporous CuO@barley straw-derived SiO_2 nanocomposite for adsorption and photocatalytic degradation of Methylene blue from real wastewater. *Colloids and Surfaces A: Physicochemical and Engineering Aspects,* 644, 1-12. DOI: 10.1016/j.colsurfa.2022.128811

[31] Zhu, L., Zhou, Y., Fei, L., Cheng, X., Zhu, X., Deng, L., Ma, X. (2022). Z-scheme CuO/Fe_3O_4/GO heterojunction photocatalyst: Enhanced photocatalytic performance for elimination of tetracycline. *Chemosphere*, 309, 1-10. DOI: 10.1016/j.chemosphere.2022.136721

[32] Nitta, R., Kubota, Y., Kishi, T., Matsushita, N. (2022). Fabrication of nanostructured CuO thin films with controllable optical band gaps using a mist spin spray technique at 90 ◦C. *Thin Solid Films*, 762, 1-7. DOI: 10.1016/j.tsf.2022.139555

[33] Hassan, J., Rajib, M.M.R., Sarker, U., Akter, M., Khan, M.N.E.A., Khandaker, S., Khalid, F., Rahman, G.K.M.M., Ercisli, S., Muresan, C.C., Marc, R.A. (2022). Optimizing textile dyeing wastewater for tomato irrigation through physiochemical, plant nutrient uses and pollution load index of irrigated soil. *Scientific Reports*, 12, 1-18. DOI: 10.1038/s41598-022-11558-1

[34] Indriyani, A., Yulizar, Y., Yunarti, R.T., Apriandanu, D.O.B., Surya, R.M. (2021). One-pot green fabrication of $BiFeO_3$ nanoparticles via Abelmoschus esculentus L. leaves extracts for photocatalytic dye degradation. *Applied Surface Science*, 563, 1-12. DOI: 10.1016/j.apsusc.2021.150113

[35] Oni, B.A., Sanni, S.E., Tomomewo, O.S., Bade, S.O. (2024). Cu_2O/SiC photocatalytic reduction of carbon dioxide to methanol using visible light on $InTaO_4$. *Materials Science in Semiconductor Processing,* 174, 108235. DOI: 10.1016/j.mssp.2024.108235

[36] Jiang, L., Ye, Q., Chen, J., Chen, Z., Gu, Y. (2018). Preparation of magnetically recoverable bentonite–Fe_3O_4–MnO_2 composite particles for Cd(II) removal from aqueous solutions. *Journal of Colloid and Interface Science*, 513, 748-759. DOI: 10.1016/j.jcis.2017.11.063

[37] Purwaningrum, W., Hasanudin, Rachmat, A., Riyanti, F., Hariani, P.L. (2023). Magnetic composite for efficient adsorption of iron and manganese ions from aqueous solution. *Ecological Engineering & Environmental Technology*, 24(8), 143-154. DOI: 10.12912/27197050/171678

[38] Shi, S., Xu, C., Dong, Q., Wang, Y., Zhu, S., Zhang, Z., Chow, Y.T., Wang, X., Zhu, L., Zhang, G., Xu, D. (2021). High saturation magnetization MnO_2/PDA/Fe_3O_4 fibers for efficient Pb(II) adsorption and rapid magnetic separation. *Applied Surface Science*, 541, 1-11. DOI: 10.1016/j.apsusc.2020.148379

[39] Abolhasani, S., Ahmadpour, A., Bastami, T.R. and Yaqubzadeh, A. (2019). Facile synthesis of mesoporous carbon aerogel for the removal of ibuprofen from aqueous solution by central composite experimental design (CCD). *Journal of Molecular Liquids*, 281, 261-268. DOI: 10.1016/j.molliq.2019.02.084

[40] Ma, Y., Wang, Q., Xing, S. (2018). Insight into the catalytic mechanism of c -Fe_2O_3/$ZnFe_2O_4$ for hydrogen peroxide activation under visible light. *Journal of Colloid and Interface Science*, 529, 247-254. DOI: 10.1016/j.jcis.2018.06.020

[41] Firmansyah, R., Bakri, R., Yulizar, Y. (2023). Enhancement of photocatalytic activity of ZnO by $ZnMoO_4$ compositing under visible light via hydrothermal green synthesis. *Inorganic Chemistry Communications*, 155, 1-10. DOI: 10.1016/j.inoche.2023.110893

[42] Reddy, K.R., Nakata, K., Ochiai, T., Murakami, T., Tryk, D.A., Fujishima, A., (2010). Nanofibrous TiO_2-Core/conjugated polymer-sheath composites: synthesis, structural properties and photocatalytic activity. *Journal of Nanoscience and Nanotechnology*, 10, 7951–7957. DOI: 10.1166/jnn.2010.3143.

[43] Yu, Z., Li, F., Yang, Q., Shi, H., Chen, Q., Xu, M., (2017). Nature-mimic method to fabricate polydopamine/graphitic carbon nitride for enhancing photocatalytic degradation performance. *ACS Sustainable Chemistry & Engineering*, 5(9), 7840-7850. DOI: 10.1021/acssuschemeng.7b01313

[44] Jia, P., Tan, H., Liu, K., Gao, W. (2018). Synthesis, characterization and photocatalytic property of novel ZnO/bone char composite. *Materials Research Bulletin*, 102, 45-50. DOI: 10.1016/j.materresbull.2018.02.018

[45] Lin, J., Luo, Z., Liu, J., Li, P. (2018). Photocatalytic degradation of methylene blue in aqueous solution by using ZnO-SnO_2 nanocomposites. *Materials Science in Semiconductor Processing*, 87, 24-31. DOI: 10.1016/j.mssp.2018.07.003

[46] Hmamouchi, S., El Yacoubi, A., El Hezzat, M., Sallek, B., El Idrissi, B.C. (2023). Optimization of photocatalytic parameters for MB degradation by g-C3N4 nanoparticles using Response Surface Methodology (RSM). *Diamond & Related Materials*, 136, 1-11. DOI: 10.1016/j.diamond.2023.109986

[47] Maleki, B., Khlaif, T.H., Jasim, M.K., Mansouri, M. (2024). Preparation and utilization of Zn-La oxide nanocatalyst as a binary composite for photocatalytic degradation of Methylene blue dye: Optimization through RSM-BBD. *Arabian Journal of Chemistry*, 17(4), 1-14. DOI: 10.1016/j.arabjc.2024.105667

[48] Hassani, A., Faraji, M., Eghbali, P. (2020). Facile fabrication of mpg-C_3N4/Ag/ZnO nanowires/Zn photocatalyst plates for photodegradation of dye pollutant. *Journal of Photochemistry and Photobiology A: Chemistry,* 400, 1-15. DOI: 10.1016/j.jphotochem.2020.112665

[49] Malika, M., Sonawane, S.S. (2021). Statistical modelling for the ultrasonic photodegradation of Rhodamine B dye using aqueous based Bi-metal doped TiO_2 supported montmorillonite hybrid nanofluid via RSM. *Sustainable Energy Technologies and Assessments*, 44, 1-15. DOI: 10.1016/j.seta.2020.100980

[50] Hasanpour, M., Motahari, S., Jing, D., Hatami, M. (2021). Statistical analysis and optimization of photodegradation efficiency of Methyl orange from aqueous solution using cellulose/zinc oxide hybrid aerogel by response surface methodology (RSM). *Arabian Journal of Chemistry*, 14, 1-13. DOI: 10.1016/j.arabjc.2021.103401

[51] Dutta, S. (2013). Optimization of Reactive black 5 removal by adsorption process using Box-Behnken Design. *Desalination and Water Treatment*, 51(40-42), 7631-7638. DOI: 10.1080/19443994.2013.779597

[52] Hariani, P.L., Said, M., Rachmat, A., Salni, S., Aprianti, N., Amatullah, A.F. (2022). Synthesis of $NiFe_2O_4/SiO_2/NiO$ Magnetic and application for the photocatalytic degradation of Methyl orange dye under UV irradiation. *Bulletin of Chemical Reaction Engineering & Catalysis*, 17(4), 699-711. DOI: 10.9767/bcrec.17.4.15788.699-711

[53] Chen, W., Xiao, H., Xu, H., Ding, T., Gu, Y. (2015). Photodegradation of Methylene blue by TiO_2-Fe_3O_4-Bentonite magnetic nanocomposite. *International Journal of Photoenergy*, 2015, 1-8. DOI: 10.1155/2015/591428

[54] Nakhaei, M., Barzgari, Z., Mohammadi, S.S., Ghazizadeh, A. (2019). Preparation of MnO_2/bentonite nanocomposite with enhanced photocatalytic activity under sunlight irradiation. *Research on Chemical Intermediates*, 45, 4995-5005. DOI: 10.1007/s11164-019-03877-2

[55] Raees, A., Jamal, M.A., Ahmed, I., Silanpaa, M., Algarni, T.S. (2021). Synthesis and characterization of CeO_2/CuO nanocomposites for photocatalytic degradation of Methylene blue in visible light. *Coatings*, 11(3), 1-11. DOI: 10.3390/coatings11030305

[56] El Khalk, A.A.A., Betiha, M.A., Mansour, A.S., El Wahed, M.G.A., Al-Sabagh, A.M. (2021). High degradation of Methylene blue using a new nanocomposite based on zeolitic imidazolate framework-8. *ACS Omega,* 20(6), 26210-26220. DOI: 10.1021/acsomega.1c03195

[57] Tripta, T., Rana, P.S. (2023). Structural, optical, electrical, and photocatalytic application of $NiFe_2O_4$@NiO nanocomposites for Methylene blue dye. *Ceramics International*, 49(9), 13520-13530. DOI: 10.1016/j.ceramint.2022.12.227

[58] Ataabadi, M.R., Jamshidi, M. (2023). Improved photocatalytic degradation of Methylene blue under visible light using acrylic nanocomposite contained silane grafted nano TiO_2. *Journal of Photochemistry & Photobiology, A: Chemistry*, 443, 3-13. DOI: 10.1016/j.jphotochem.2023.114832

[59] Yadav, S., Kumar, A., Kumar, D. (2023). Photo degradation of Methylene blue onto boron/phosphorous modified carbons dots prepared by hydrothermal and microwave assisted methods. *Materials Science for Energy Technologies*, 6, 260-266. DOI: 10.1016/j.mset.2023.01.003

[60] Kalycioglu, Z., Uysal, B.O., Pekcan, O., Erim, F.B. (2023). Efficient photocatalytic degradation of Methylene blue dye from aqueous solution with cerium oxide nanoparticles and graphene oxide-doped polyacrylamide. *ACS Omega*, 8(14), 13004-13015. DOI: 10.1021/acsomega.3c00198

[61] Ao, Y., Xu, J., Fu, D., Shen, X., Yuan, C. (2008). Low temperature preparation of anatase TiO_2-coated activated carbon. *Colloids and Surfaces A: Physicochemical and Engineering Aspects,* 312(2-3), 125-130. DOI: 10.1016/j.colsurfa.2007.06.039

[62] Ichipi, E.O., Mapossa, A.B., Costa, A.C.F.M., Chirwa, E.M.N., Tichapondwa, S.M. (2023). Fabrication and characterization of recyclable, magnetic $(CoFe_2O_4)x/Ag_2S$-ZnO composites for visible-light-induced photocatalytic degradation of Methylene blue dye. *Journal of Water Process Engineerin*, 54, 1-15. DOI: 10.1016/j.jwpe.2023.104040

[63] Elviera, E., Yulizar, Y., Apriandanu, D.A.B., Surya, R.M. (2022). Fabrication of novel $SnWO_4$/ZnO using *Muntingia calabura* L. leaf extract with enhanced photocatalytic Methylene blue degradation under visible light irradiation. *Ceramics International*, 48, 3564-3577. DOI: 10.1016/j.ceramint.2021.10.135